Chemical Engineering Journal 165 (2010) 735–739

Contents lists available at ScienceDirect

Chemical Engineering Journal

journal homepage: www.elsevier.com/locate/cej

High photocatalytic activity of Zn_2SnO_4 among various nanostructures of $Zn_{2x}Sn_{1-x}O_2$ prepared by a hydrothermal method

Azam Anaraki Firooz[a,*], Ali Reza Mahjoub[a,*], Abbas Ali Khodadadi[b,c], Maryam Movahedi[d]

[a] Department of Chemistry, Tarbiat Modares University, 14115-175 Tehran, Iran
[b] School of Chemical Engineering, University of Tehran, 11155-4563 Tehran, Iran
[c] Nanoscience and Nanotechnology Research Center of University of Tehran, Iran
[d] Department of Chemistry, Payame Noor University (PNU), P.O. Box 81395-671 Isfahan, Iran

ARTICLE INFO

Article history:
Received 15 May 2010
Received in revised form 29 August 2010
Accepted 10 September 2010

Keywords:
Zn_2SnO_4
Hydrothermal
Photocatalytic activity
Photoluminescence property

ABSTRACT

Different structures and morphologies of SnO_2 containing various amounts of ZnO were synthesized via a hydrothermal method (without any template), characterized by scanning electron microscopy and powder X-ray diffraction, and used for photocatalytic degradation of Congo red. The results revealed that using different ratios of Zn^{+2}/Sn^{+2} affects the phase and morphology of the $Zn_{2x}Sn_{1-x}O_2$ compounds. This type of tailoring the morphology of SnO_2 nanoparticles, ZnO doped SnO_2 porous structure, $ZnSnO_3$ flower-like, and Zn_2SnO_4 octahedrals was possible, by varying the Zn^{+2}/Sn^{+2} ratio of 0, 1/10, 1/5 and 1/1, respectively. The formation mechanism of these products was proposed. Zn_2SnO_4 with octahedral morphology exhibited a significant enhancement of photocatalytic activity toward degrading Congo red, as compared to other samples. This could be attributed to enhanced oxygen vacancies and crystallite defects formed by substitution of Zn^{+2} in the lattice of SnO_2, revealed in photoluminescence measurements.

1. Introduction

In recent years, heterogeneous photocatalysis has received increasing attention for environmental applications such as air purification, water disinfection, hazardous remediation and water purification [1–3]. The high photocatalytic degradation of semiconductors, such as TiO_2 and ZnO has attracted extensive attention of many researchers [4,5]. In such semiconductors, photogenerated carriers (electrons and holes) could tunnel to a reaction medium and participate in chemical reactions. The high degree of recombination of these carriers decreased greatly their photocatalytic efficiency. Clearly, a wider separation of the electron and the holes increases the efficiency of photocatalyst. Furthermore, oxygen vacancies and defects strongly influence photocatalytic reactions [6]. Fortunately, utilization of multifunctional materials could increase the charge separation and oxygen vacancies and extend the energy range of photooxidation [7]. By far, many research groups have carried out the photocatalytic activity experiments of various coupled semiconductors [8–11]. Among the coupled semiconductors, ZnO and SnO_2, well-known n-type semiconductors, have been considered due to their highly sensitive gas sensing and excellent optical properties [12–15].

In this paper, we demonstrate a facile hydrothermal method for synthesizing various $Zn_{2x}Sn_{1-x}O_2$ structures and morphologies by changing the Zn^{+2}/Sn^{+2} ratios. Zn_2SnO_4 with octahedral morphology showed enhanced photocatalytic efficiency for degrading Congo red.

2. Experimental

2.1. Hydrothermal synthesis

All chemicals (analytical grade) were purchased from Merck and used as received without further purification. In this paper, the samples were synthesized by using a hydrothermal method. Experimental details were as follows: firstly, $SnCl_2{\cdot}2H_2O$ (3 mmol) was dissolved in 20 mL of distilled water. Secondly, 20 mL NaOH (1 M) solution was slowly dropped into the above solution under magnetic stirring. Thirdly, the solution containing $ZnCl_2$ (0.3, 0.6 or 3 mmol) was introduced to the above solution drop by drop under stirring. Lastly, the white slurry was transferred into a 200 mL Teflon-lined stainless autoclave. The autoclave was sealed and maintained in a furnace at 200 °C for 48 h and then passively cooled down to room temperature. The obtained white precipitate was filtered off, washed several times in distilled water and absolute ethanol, and dried in air at room temperature.

* Corresponding authors. Tel.: +98 2182883442; fax: +98 2182883455.
E-mail addresses: azam_a_f@yahoo.com (A.A. Firooz), Mahjouba@modares.ac.ir (A.R. Mahjoub).

1385-8947/$ – see front matter © 2010 Elsevier B.V. All rights reserved.
doi:10.1016/j.cej.2010.09.052

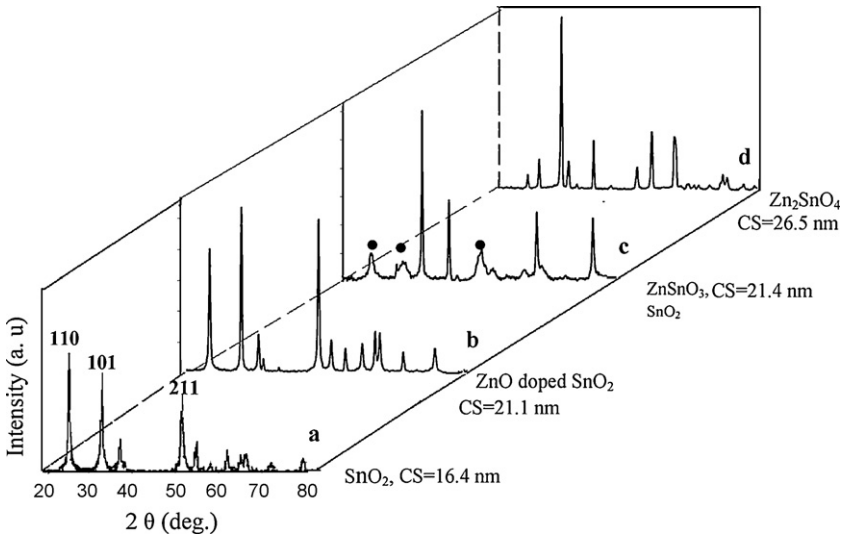

Fig. 1. XRD patterns of samples (the marked peaks are attributed to SnO_2 phase), along with their crystallite sizes (CS).

2.2. Characterizations

The products were characterized using scanning electron microscopy (SEM) of a Holland Philips XL30 microscope. To protect samples from charging by the electron beam, during observation, the samples were coated with the thin gold film. XRD patterns of these products were recorded in ambient air using a Holland Philips Xpert X-ray powder diffraction (XRD) (Cu Kα, λ = 1.5406 Å), at scanning speed of 0.2°/min from 20° to 80° (2θ).

Average crystallite sizes of products were calculated using Scherrer's formula: $D = 0.9\lambda/\beta \cos\theta$ [13], where D is the diameter of the nanoparticles, λ (Cu Kα) = 1.5406 Å and β is the full-width at half-maximum of the diffraction lines.

The photoluminescence (PL) spectrum was recorded by applying a Hitachi (850) fluorescence spectrophotometer at room temperature.

2.3. Evaluation of photocatalytic activity

First, the solution of 5 ppm (w/v) Congo red (C.I. Direct Red 28, M.W. = 696.67 g/mol $C_{32}H_{24}N_6O_6S_2{\cdot}2Na$) was prepared by its dissolving in distilled water. The photocatalysis experiments were carried out in beaker containing about 50 mL of Congo red aqueous solution and about 0.025 g of $Zn_{2x}Sn_{1-x}O_3$ compounds as photocatalyst. A UV lamp (30W, UV-C, λ = 253.7 nm, photon provides 4.89 eV, manufactured by Philips, Holland) irradiated perpendicularly to the surface of solution and distance between the UV source and vessel containing reaction mixture was fixed at 15 cm. Air was blown into the reaction by an air pump, to maintain the solution saturated with oxygen during the course of the reaction. During irradiation, agitation was maintained by a magnetic stirrer to keep the suspension homogeneous, the suspension was sampled after regular intervals and immediately centrifuged at 3500 rpm for 4 min to completely remove catalyst particles.

The progress of photocatalytic degradation was monitored by Chemical Oxygen Demand (COD) analysis which was measured by the dichromate reflux method [16]. The concentration of the solution samples was measured by UV–vis spectrophotometer (Shimadzu UV 2100).

Absorption peaks corresponding to Congo red appeared at 497, 347 and 237 nm. The concentration of dye in each degraded sample was determined at λ_{max} = 497 nm, using a calibration curve. By this method conversion percent of Congo red azo dye can be obtained in different intervals. The degree of photodecolorization (X) is given by:

$$X = (C_0 - C)/C_0 \quad (1)$$

In where, C_0 is the initial concentration of dye and C is the concentration of dye at different times.

3. Results and discussion

XRD patterns of the samples are shown in Fig. 1a–d. According to the JCPDS file no. 41-1445, all XRD peaks in Fig. 1a and 1b for SnO_2 and ZnO doped SnO_2 (Zn^{+2}/Sn^{+2} = 1/10), respectively, fit well the tetragonal rutile structure of SnO_2 with no peak of ZnO crystalline phase or impurities. It seems that the substitution of Zn^{2+} into tetravalent tin increase the crystal polarity due to the similar ionic radius and different charges. So, when small quantities of zinc ions were incorporated into the crystal lattice of tin dioxide, doped SnO_2 crystal will have some polarity due to the diversity of the crystal texture of ZnO and SnO_2 [17]. Therefore, regarding to dramatic enhancement of the peak intensity of (1 0 1) plane relative to (1 0 0) plane, zinc ions in SnO_2 may guide SnO_2 nanocrystals growth along (1 0 1) orientation.

The calculated crystallite sizes of the samples by the Scherrer's formula were shown in Fig. 1. The data shows that the crystallite size increases with the addition of Zn^{+2}.

When the molar ratio of Zn^{+2}/Sn^{+2} increased to 1/5 (Fig. 1c), another phase, $ZnSnO_3$ (JCPDS file No. 11-0274), besides the rutile phase of SnO_2 crystals was observed in its XRD pattern. Also, when the molar ratio of Zn^{+2}/Sn^{+2} was further increased to 1/1, Zn_2SnO_4 (JCPDS file No. 14-0381) was obtained (see Fig. 1d).

The morphologies of the products were examined by SEM. Fig. 2 shows the typical SEM images of the samples obtained by the hydrothermal method with different molar ratio of Zn^{+2}/Sn^{+2}. As shown in Fig. 2a–d, when only Sn^{+2} was used, SnO_2 nanoparticles were formed. Porous morphology was formed at lower Zn^{+2}/Sn^{+2} ratio of 1/10. When the molar ratio of Zn^{+2}/Sn^{+2} was 1/5, a mixture of SnO_2 and $ZnSnO_3$ with a flower-like morphology was obtained. Finally, with increasing of Zn^{+2}/Sn^{+2} ratio to 1/1, Zn_2SnO_4 with morphology of octahedral was observed to form. The results revealed that the introduction of Zn^{2+} can play an important role in directing the growth of SnO_2 crystals and formation of different phases and morphologies. In the initial stage of the hydrothermal reaction, some complexes such as $Sn(OH)_6^{2-}$, $ZnSn(OH)_6$, and $Zn(OH)_4^{2-}$ are

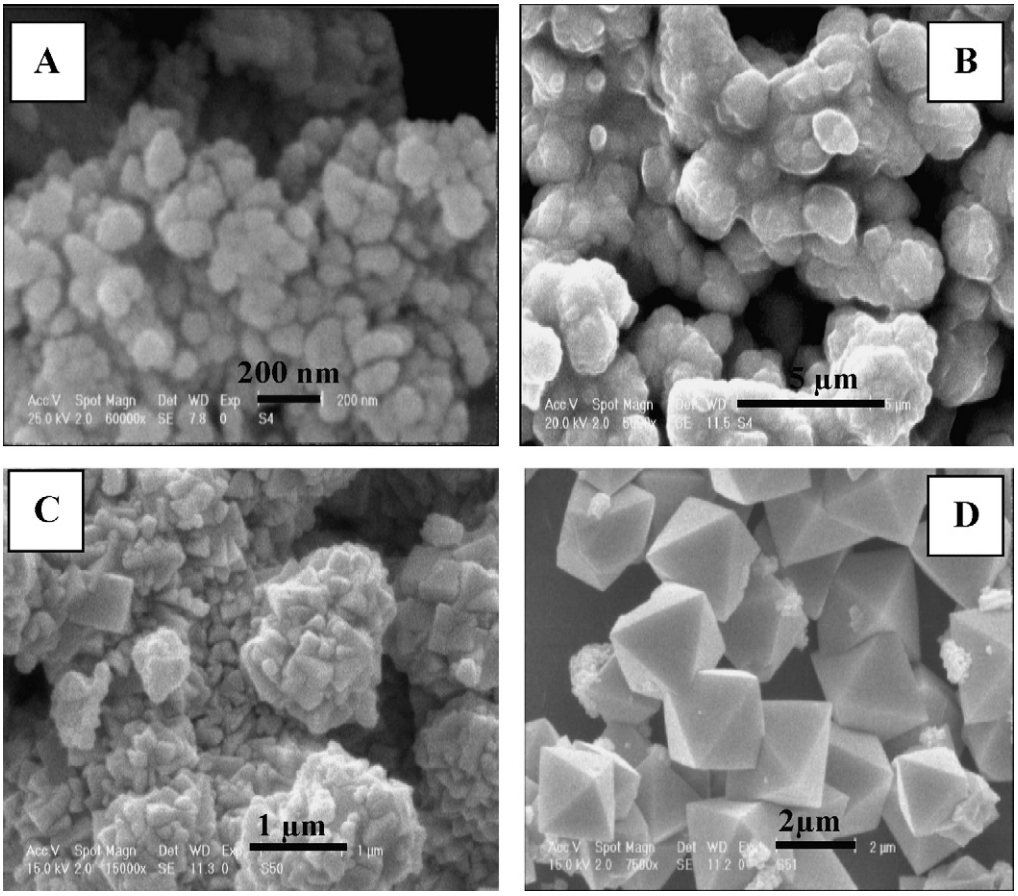

Fig. 2. SEM images of samples (a) SnO_2 nanoparticles, (b) ZnO doped SnO_2 porous structure, (c) $ZnSnO_3$ flower-like, (d) Zn_2SnO_4 octahedral.

formed in the presence of NaOH [18]. At the same time, with decomposition of $Sn(OH)_6^{2-}$, SnO_2 nuclei would form and attach to the surface of the $ZnSn(OH)_6$ spheres. Furthermore, high temperature and high pressure of hydrothermal treatment lead to decompose of these complexes. As a result, the SnO_2 crystal growth process is accomplished by decomposition of $ZnSn(OH)_6$ phase. Probably this process can be attributed to the following mechanism [19]:

$$Zn^{2+} + Sn(OH)_6^{2-} \leftrightarrow Zn[Sn(OH)_6] \quad (2)$$

$$Zn^{2+} + 4OH^- \leftrightarrow Zn(OH)_4^{2-} \quad (3)$$

$$Sn(OH)_6^{2-} \leftrightarrow SnO_2 + 2OH^- + 2H_2O \quad (4)$$

$$2xZn[Sn(OH)_6] + (1-3x)Sn(OH)_6^{2-} \leftrightarrow Zn_{2x}Sn_{(1-x)}O_2 + (2-6x)OH^- + 2H_2O \quad (5)$$

It is well known that the ionic radius of Zn^{2+} (0.74 Å) is close to that of Sn^{4+} which can easily replace in the lattice of SnO_2. On the other hand, with increasing the molar ratio of Zn^{+2}/Sn^{+2}, other crystal phases as $ZnSnO_3$ and Zn_2SnO_4 were obtained. However, the exact growth mechanism is not clear and needs further investigation.

The photocatalytic activities of SnO_2 nanoparticles, ZnO doped SnO_2 porous structure, $ZnSnO_3$ flower-like and Zn_2SnO_4 octahedral were further investigated by the photodegradation of Congo red dye under UV irradiation; the results of last three samples are presented in Fig. 3. The results show that the morphology and phase of the photocatalyst have obvious influence on the degradation of the reactive dyestuff.

Congo red with N=N azo group (Scheme 1) yields gaseous dinitrogen under photocatalytic conditions [20]. It was strongly adsorbed on photocatalyst surfaces through the two oxygen atoms of the sulfonate group of the dye molecules [21]. After UV light illumination, the intensity of the absorption bands of the dye in the visible region decreases with increasing time and, finally disappears, indicating the destruction of its chromophoric structure in the vicinity of the azo-linkage. This is accompanied by a parallel decrease of the intensities of the bands in the ultraviolet region located at 235 and 347 nm, attributed to the benzoic and naphthalene rings, respectively. These aromatic rings convert to hydroxylated metabolites, when photogenerated •OH radicals attacks to them.

As expected from the photocatalytic results, the intensity of the visible light chromophore band of Congo red (azo-linkage)

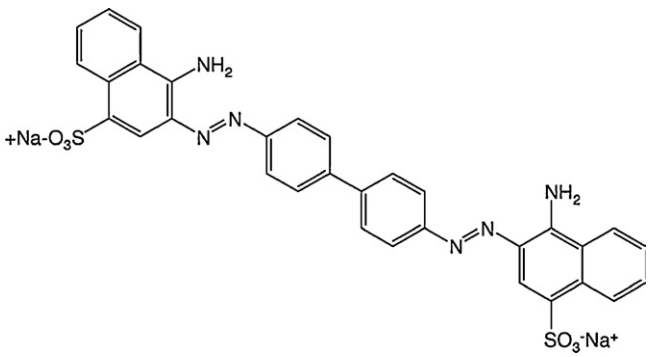

Scheme 1. Structure of Congo red (C.I. Direct Red 28).

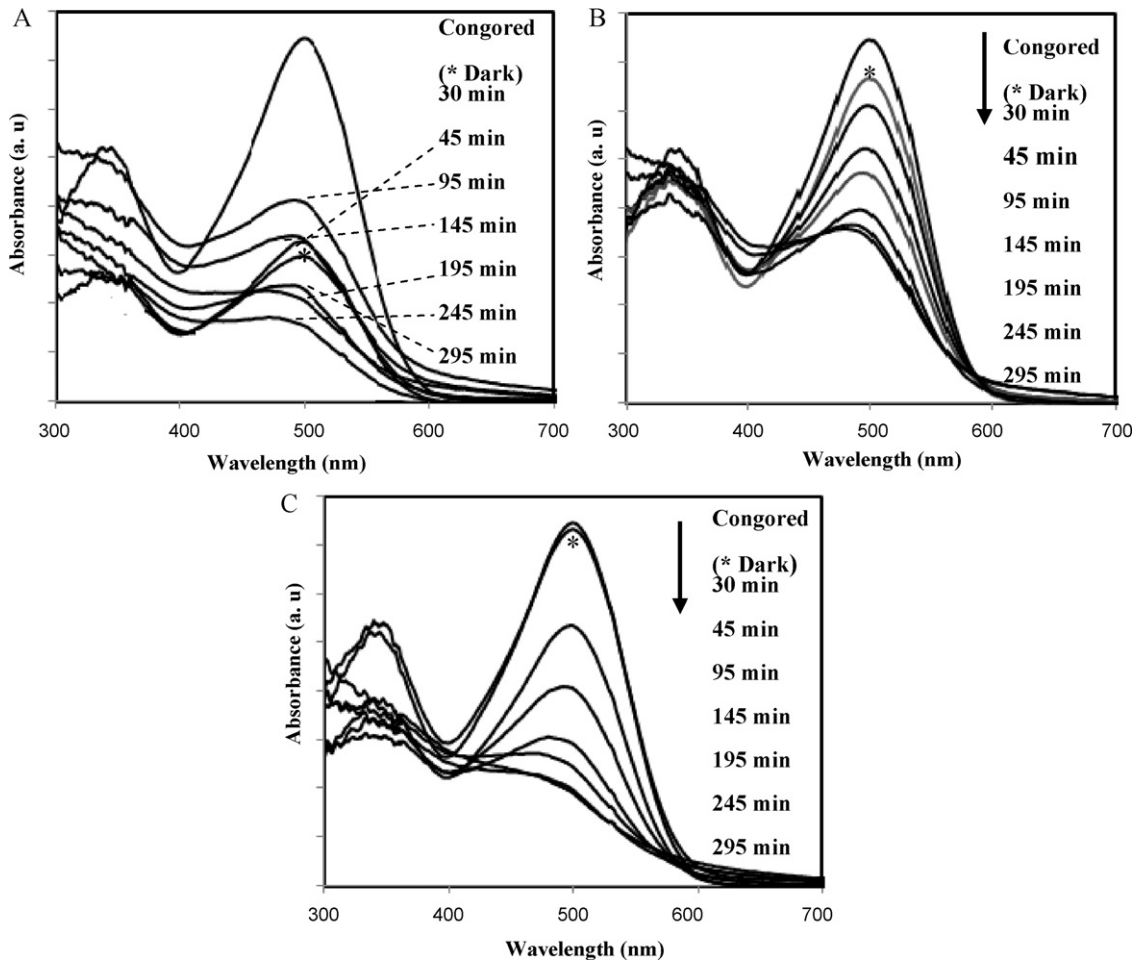

Fig. 3. Absorbance spectral changes of Congo red solution in the presence of (A) ZnO doped SnO_2 porous structure, (B) $ZnSnO_3$ flower-like, (C) Zn_2SnO_4 octahedral.

decreased as a function of time, resulting in decolorization or mineralization of the solution, based on UV–vis spectra and COD value. COD values have been related to the total concentration of organics in the solution and their decrease reflects the degree of mineralization.

When the photocatalysts were applied in the dark condition for 30 min, the concentrations of Congo red in the case of ZnO doped SnO_2 decreased remarkably, which is due to the adsorption of dye molecule on the surface of photocatalyst, and then desorption Congo red was occurred after 45 and 95 min UV irradiation (Fig. 3A). The absorbance of many dye molecules on the surface of this photocatalyst can be attributed to its special morphology. In contrast, Congo red molecules could not be adsorbed on SnO_2 nanoparticles and Zn_2SnO_4 photocatalysts under the dark condition. $ZnSnO_3$ photocatalyst adsorbs about 10% of dye molecules. Fig. 4 shows adsorption behavior of the samples in dark conditions. In the presence of Zn_2SnO_4 and light, the degradation of dye increases quickly with irradiation time in comparison with other photocatalysts (Fig. 5).

It is well known that Zn_2SnO_4 with spinel-type structure is an n-type semiconductor with oxygen deficiency Zn_2SnO_{4-X} structure deficient [19]. So the increased activity of Zn_2SnO_4 for dye molecules degradation can be attributed to the presence of a large content of oxygen vacancies in this photocatalyst. When Zn_2SnO_4 is in equilibrium with O_2, the defect reactions take places as follows [22]:

$$2O_O^x \leftrightarrow 2V_O^{\bullet\bullet} + 4e + O_2\uparrow \quad (6)$$

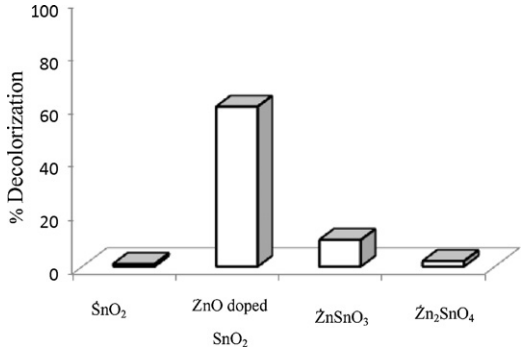

Fig. 4. Adsorption behavior of the samples in dark conditions.

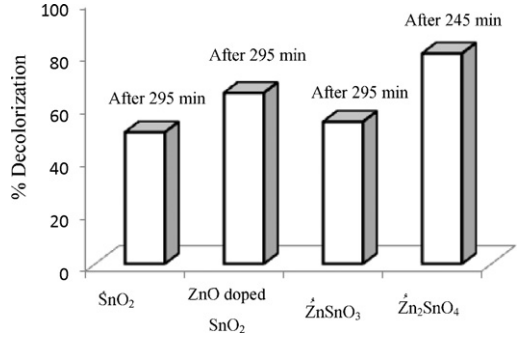

Fig. 5. Photocatalytic results of the samples after UV light irradiations.

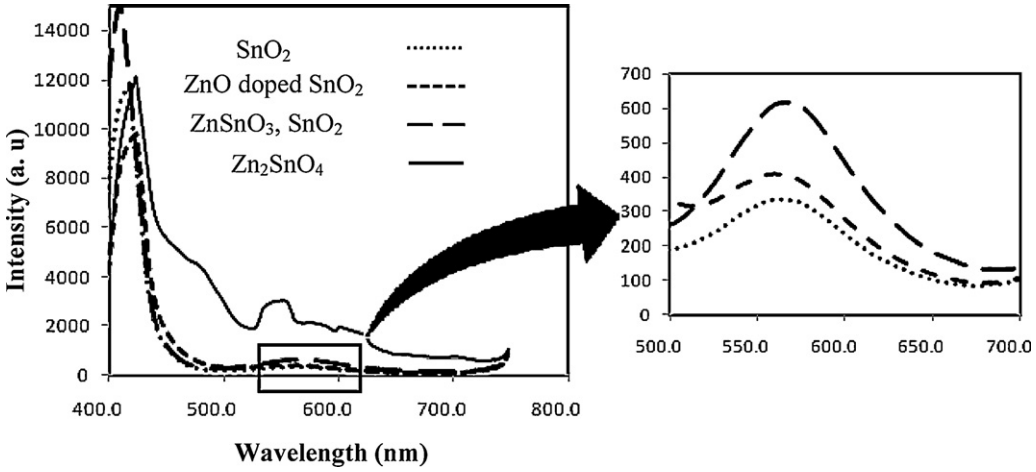

Fig. 6. The PL spectra of the samples.

In where, O_O^x is lattice oxygen and $V_O^{\bullet\bullet}$ is oxygen vacancies with double positive charges.

When oxygen vacancies are formed and the density of reactive OH^- becomes higher, photocatalytic reaction is facilitated. After UV irradiation, the particles produce high-energy electron–hole pairs according to the following reaction:

$$Zn_2SnO_4 + h\upsilon \rightarrow Zn_2SnO_4{}^*(e_{CB}{}^- + h_{VB}{}^+) \quad (7)$$

where, $e_{CB}{}^-$ is produced electron in conductive band and $h_{VB}{}^+$ is produced hole in valance band.

These electron–hole pairs react with water and dissolve oxygen to produce $^\bullet OH$ free radicals with high chemical activity, and react with the dyes molecule adsorbed on the surface of Zn_2SnO_4 photocatalyst. Thus the dyes molecule will be photodegradated because the oxidation–reduction reaction happens.

The PL spectrum of these samples was measured at room temperature and the excitation wavelength was 380 nm. As shown in Fig. 6, there is a strong peak at about 410–420 nm in all samples. A weak shoulder at about 470 nm is also observed for Zn_2SnO_4. In comparison with other reports [23], these observed peaks might result from other luminescence centers, such as oxygen vacancies and crystal defects. A broad green emission band centered at 560 nm is observed in the spectrum of the SnO_2 nanoparticles, ZnO doped SnO_2 and $ZnSnO_3$ and that centered at 535 nm is also observed in the spectrum of Zn_2SnO_4. Compared with standard peak of SnO_2 powder at 575 nm [24], the peak position of Zn_2SnO_4 has a blue shift of approximately 40 nm, while the peak positions of the SnO_2 nanoparticles, ZnO doped SnO_2 and $ZnSnO_3$ shows a blue shift of approximately 15 nm. It is well known that the morphology, size and nature of materials have a great influence on the PL properties. These PL peaks and their blue shift may be related to crystalline defects during the growth course, substitution of Zn^{+2} in the lattice of SnO_2 and the nature of phase.

Also, Zn_2SnO_4 shows an orange-yellow band at about 603 nm that is similar with that of the reported Zn_2SnO_4 microcrystal [23]. This result indicates that besides oxygen-vacancy emission, there may be other luminescence centers in Zn_2SnO_4 due to the interactions between oxygen vacancies and interstitial tin or zinc vacancies, and result in the specific PL signals of Zn_2SnO_4. Thus, high photocatalytic activity of Zn_2SnO_4 can be attributed to the large content of oxygen vacancies and crystalline defects.

4. Conclusion

In summary, SnO_2 nanoparticles, ZnO doped SnO_2 porous structure, $ZnSnO_3$ flower-like and Zn_2SnO_4 octahedral structures were successfully synthesized by a simple template-free hydrothermal method. Morphologies and phases of the nanostructures obtained are strongly affected by the molar ratio of Zn^{2+} and Sn^{2+}. Among the various morphologies and phases, Zn_2SnO_4 octahedral shows the highest photocatalytic activity for degradation of Congo red. PL spectrum of this sample shows that there are oxygen vacancies and crystalline defects that may be responsible for the high photocatalytic activity of Zn_2SnO_4 photocatalyst.

Acknowledgment

We gratefully acknowledge the financial support of the Tarbiat Modares University and Nanoscience and Nanotechnology Research Center of University of Tehran.

References

[1] A. Fujishima, T.N. Rao, D.A. Tryk, J. Photochem. Photobiol. C: Photochem. 1 (2000) 1–21.
[2] B. Pal, T. Hata, K. Goto, G. Nogami, J. Mol. Catal. A: Chem. 169 (2001) 147–155.
[3] J.C. Yu, J. Lin, R.W.M. Kwok, J. Phys. Chem. B 102 (1998) 5094–5098.
[4] H. Lachheb, E. Puzenat, A. Houas, M. ksibi, E. Elaloui, C. Guillard, et al., Appl. Catal. B: Environ. 39 (2002) 75–90.
[5] K. Tennakone, J. Bandara, Appl. Catal. A: Gen. 208 (2001) 335–341.
[6] N. Serpone, P. Maruthamuthu, P. Pichat, E. Pelizzetti, H. Hidaka, J. Photochem. Photobiol. A: Chem. 85 (1995) 247–255.
[7] X. Lou, X. Jia, J. Xu, S. Liu, Q. Gao, Mater. Sci. Eng. A 432 (2006) 221–225.
[8] W. Cun, X.M. Wang, B.Q. Xu, J.C. Zhao, B.X. Mai, P. Peng, G.Y. Sheng, H.M. Fu, J. Photochem. Photobiol. A 168 (2004) 47–52.
[9] L. Shi, Y. Xu, S. Hark, Y. Liu, S. Wang, L.-M. Peng, K. Wong, Q. Li, Nano Lett. 7 (2007) 3559–3563.
[10] Z. Wen, G. Wang, W. Lu, Q. Wang, Q. Zhang, J. Li, Cryst. Growth Des. 7 (2007) 1722–1725.
[11] C. Wang, B.-Q. Xu, X. Wang, J. Zhao, J. Solid State Chem. 178 (2005) 3500–3506.
[12] A. Anaraki Firooz, A.R. Mahjoub, A.A. Khodadadi, Mater. Chem. Phys. 115 (2009) 196–199.
[13] A. Anaraki Firooz, A.R. Mahjoub, A.A. Khodadadi, Sens. Actuators B: Chem. 141 (2009) 89–96.
[14] A. Anaraki Firooz, A.R. Mahjoub, A.A. Khodadadi, Mater. Lett. 62 (2008) 1789–1792.
[15] J. Zhang, L. Sun, J. Yin, H. Su, C. Liao, C. Yan, Chem. Mater. 14 (2002) 4172–4177.
[16] APH/AWWA/WPCF, Standards Methods for the Examination of Water and Wastewater, 17th ed., American Public Health Association, Washington, DC, 1989.
[17] Z. Li, X. Li, X. Zhang, Y. Qian, J. Cryst. Growth 291 (2006) 258–261.
[18] W.-W. Wang, Y.-J. Zhu, L.-X. Yang, Adv. Funct. Mater. 17 (2007) 59–64.
[19] G. Cheng, K. Wu, P. Zhao, Y. Cheng, X. He, K. Huang, J. Cryst. Growth 309 (2007) 53–59.
[20] H. Lachheb, E. Puzenat, A. Houas, M. Ksibi, E. Elaloui, C. Guillard, J.M. Herrmann, Appl. Catal. B: Environ. 39 (2002) 75–90.
[21] M. Movahedi, A.R. Mahjoub, S. Janitabar-Darzi, J. Iran. Chem. Soc. 6 (2009) 570–577.
[22] C. Wang, X. Wang, J. Zhao, B. Mai, G. Sheng, P. Peng, J. Fu, J. Mater. Sci. 37 (2002) 2989–2996.
[23] J. Hu, Y. Bando, Q. Liu, D. Golberg, Adv. Funct. Mater. 13 (2003) 493–496.
[24] J.-W. Zhao, L.-R. Qin, L.-D. Zhang, Solid State Commun. 141 (2007) 663–666.